Intracellular amorphous calcium carbonate biomineralization in methanotrophic gammaproteobacteria was acquired by horizontal gene transfer from cyanobacteria

Running title: ACC biomineralization in aerobic methanotrophs

Benzerara Karim[1], Millet Maxime[1], Skouri-Panet Fériel[1], Gaschignard Geoffroy[1], Mehta Neha[1], Bezard Malo[1], Caumes Geraldine[1], Chevrier Daniel M.[2], Dezi Manuela[1], Duverger Arnaud[1], Guigner Jean-Michel[1], Gutiérrez-Preciado Ana[3], Lefevre Christopher T.[2], López-García Purificación[3], Menguy Nicolas[1], Monteil Caroline L.[2], Pehau-Arnaudet Gerard[4], Penard Esthel[4], Pereiro Eva[5], Scandola Cyril[4], Travert Cynthia[1], Vantelon Delphine[6], Duprat Elodie[1], Callebaut Isabelle[1], Moreira David[3]

[1]Sorbonne Université, Muséum National d'Histoire Naturelle, UMR CNRS 7590. Institut de Minéralogie, de Physique des Matériaux et de Cosmochimie (IMPMC), 75005 Paris, France.

[2]Aix-Marseille Université, CEA, CNRS, BIAM, UMR7265, Institut de Biosciences et Biotechnologies Aix-Marseille, CEA Cadarache, F-13115, Saint-Paul-lez-Durance, France

[3]Unité d'Ecologie Société et Evolution, CNRS, Université Paris-Saclay, AgroParisTech, Gif-sur-Yvette, France

[4]Institut Pasteur, Université Paris Cité, Ultrastructural Bioimaging Unit, 75015 Paris, France

[5]ALBA Synchrotron Light Source, Cerdanyola del Vallés, Barcelona 08290, Spain

[6]Synchrotron SOLEIL, L'Orme des Merisiers, 91190 Saint-Aubin, France

For correspondence: karim.benzerara@sorbonne-universite.fr

Keywords

Amorphous calcium carbonate; methanotrophs; Cyanobacteria; biomineralization; horizontal gene transfer

Abstract

Some bacteria genetically control the biomineralization of intracellular amorphous calcium carbonates (iACC) with potential implications for microbial physiology, evolution, bioremediation and biogeochemical cycling. Until now, this capacity has been documented in *Cyanobacteria*, the giant gammaproteobacterium *Achromatium* and a few magnetotactic *Pseudomonadota*. Here, we report the discovery of iACC biomineralization in members of the *Methylococcaceae*, a family of aerobic methanotrophic *Gammaproteobacteria*. A homolog of the *ccyA* gene, previously considered a diagnostic marker for iACC formation in *Cyanobacteria*, was identified in several *Methylococcaceae* genomes. Moreover, two cultivated strains, *Methylococcus geothermalis* and *Methylococcus mesophilus*, were consistently shown to form iACC granules. The *ccyA* genes in *Methylococcaceae* and *Microcystis* share stronger sequence and structural similarities than with other *Cyanobacteria*, suggesting horizontal gene transfer (HGT) from an ancestral *Microcystis*-like cyanobacterium to *Methylococcaceae*. This finding extends the known taxonomic distribution of *ccyA* and indicates that the capability to biomineralize iACC was acquired by HGT, possibly in environments such as lakes, where *Cyanobacteria* and *Methylococcaceae* commonly co-exist. The discovery of iACC in methane-oxidizing *Methylococcaceae* highlights a previously unrecognized coupling between calcium carbonate biomineralization and methane cycling in aquatic environments, suggesting that iACC formation may play an overlooked role in microbial carbon storage and local geochemical regulation.

1. Introduction

Many bacteria are capable of forming a wide range of mineral phases through a process known as biomineralization. This process may serve specific biological functions such as protection, detoxification, assistance in cell movements or storage (Cosmidis and Benzerara, 2022) and has

54 a significant impact on both local and global geochemical cycles, inspiring a variety of
55 applications (Qin et al., 2020; Wan et al., 2024; Zhang et al., 2023). Among biomineralizing
56 bacteria, several phylogenetically diverse species have been shown to form intracellular
57 amorphous calcium carbonates (iACC). The giant gammaproteobacterium *Achromatium*
58 *oxaliferum* was the first such organism discovered, as early as the late 19th century
59 (Schewiakoff, 1893). For a long time, it remained the only known iACC-biomineralizing
60 bacterium (Benzerara et al., 2021; Gray, 2006). However, since 2012, diverse cyanobacteria
61 have also been found to form iACC (Benzerara et al., 2014, 2022; Couradeau et al., 2012).
62 More recently, additional members of the *Pseudomonadota* and *Nitrospirota*, including
63 magnetotactic bacteria capable of biomineralizing intracellular magnetite crystals (Fe(II)-
64 Fe(III) oxides), have been shown to form iACC as well (Liu et al., 2021, 2025; Mangin et al.,
65 2025; Monteil et al., 2020). This rapidly expanding diversity of iACC-forming bacteria suggests
66 that many more such organisms likely remain to be discovered.

67 Forming iACC granules incurs an energy cost to cells, at least under certain conditions (Cam
68 et al., 2017), suggesting that these granules likely confer adaptive benefits to the cells. However,
69 their exact biological role remains poorly understood (Cosmidis and Benzerara, 2022). Some
70 studies have proposed that iACC granules may buffer intracellular pH fluctuations, serve as
71 carbon reservoirs, or act as ballast for the cells (Görgen et al., 2020). Regardless of their specific
72 function, iACC granules involve a particular Ca homeostasis in the cells that form them,
73 including Ca exchange between the cells and the surrounding solution with a net inward influx
74 (Benzerara et al., 2023; Mehta et al., 2023, 2024). Studying these granules offers valuable
75 insights: (i) Amorphous calcium carbonate (ACC) is essential to many $CaCO_3$-biomineralizing
76 eukaryotes (Gilbert et al., 2022), and the ability to form iACC may have originated early in
77 evolutionary history within prokaryotes before being transferred to eukaryotes (Ponce-Toledo
78 et al., 2017). Testing this hypothesis requires further exploration of the evolutionary links

between iACC formation across different bacterial lineages. (ii) iACC-forming bacteria can influence the local geochemical cycling of alkaline earth metals (Ca, Sr, Ba), particularly when they bloom as large populations (Blondeau et al., 2018b; Gaetan et al., 2023). Last, (iii) some of these bacteria are capable of sequestering toxic radioisotopes, opening new avenues for the development of bioremediation strategies (Mehta et al., 2019, 2022a; Pamart et al., 2025).

Despite the significance of this biomineralization process, the molecular mechanisms underlying bacterial iACC formation remain largely unexplored. In *Cyanobacteria*, iACC forms within envelopes thought to consist of proteins and/or lipid monolayers (Blondeau et al., 2018a). Through comparative genomics, a novel gene family named *ccyA* was identified (Benzerara et al., 2022). This gene family lacks homologs with a known function but serves as a diagnostic marker for iACC formation in *Cyanobacteria*. The *ccyA* gene encodes two-domain proteins, the calcyanins, with a C-terminal domain conserved across cyanobacterial clades, composed of several long glycine zipper (Gly-zip) motifs, and a variable N-terminal domain that defines four distinct calcyanin subgroups, corresponding to different *Cyanobacteria* clades (Benzerara et al., 2022). Interestingly, the N-terminal domain of one calcyanin subgroup contains a CoBaHMA domain, which is hypothesized to play a regulatory role, possibly interacting with anionic lipids (Gaschignard et al., 2024). Furthermore, a recent study suggests that other genes may operate in concert with *ccyA*, such as a *cax* gene encoding a Ca^{2+}/H^{+} transporter (Bruley et al., 2025).

In this study, we report the discovery of a homolog of the *ccyA* gene in *Methylococcaceae*, a family of *Gammaproteobacteria*. Furthermore, two cultivated strains from this family were found to form iACC, providing evidence that *ccyA* is a marker of iACC biomineralization beyond the *Cyanobacteria* phylum. The phylogenetic distribution of *ccyA* within

102 *Methylococcales*, along with its comparison with the *ccyA* genes in *Cyanobacteria*, offer new
103 insights into the evolutionary origins of iACC biomineralization in *Methylococcaceae*.

104

105 ## 2. Materials and methods

106 ### 2.1 Bacterial strains

107 The strain *Methylococcus geothermalis* IM1 (=JCM 33941 =KCTC 72677) was ordered from
108 the Riken bioresource research center in Japan (https://www.jcm.riken.jp/cgi-
109 bin/jcm/jcm_number?JCM=33941. *M. geothermalis* is an aerobic, planktonic and non-motile,
110 methanotroph isolated from a hot spring soil in Korea (Awala et al., 2020). Here, it was cultured
111 in triplicates at 37 °C in 10 mL of modified nitrate mineral salts medium-2 (M1221;
112 https://www.jcm.riken.jp/cgi-bin/jcm/jcm_grmd?GRMD=1221) in a 120-mL glass serum
113 bottle with a 25-75 vol% of CH_4-air mix in the headspace. The genome sequence is available
114 under NCBI accession number CP046565.1.
115 The strain *Methylococcus mesophilus* 16-5^T (=KCTC 82050^T) was provided by Dr. Samuel
116 Imisi Awala from University of Calgary. *M. mesophilus* is a mesophilic, aerobic methanotroph
117 isolated from a rice field in Korea (Awala et al., 2023). It was cultured in triplicates at 21°C in
118 10 mL of modified nitrate mineral salts medium-2 (M1221; https://www.jcm.riken.jp/cgi-
119 bin/jcm/jcm_grmd?GRMD=1221) in a 120-mL glass serum bottle with a 25-75 vol% of CH_4-
120 air mix in the headspace. The genome sequence is available under NCBI accession number
121 CP110921.1.
122 Cell growth for both strains was assessed by measuring optical density at 600 nm. The pH of
123 the cell suspension was measured over the growth of the cells with a precision better than 0.1.

124

125 ### 2.2 Fourier Transform infrared spectroscopy (FTIR)

126 FTIR spectroscopy analyses of both strains were performed to detect bulk signals from iACC
127 inclusions, following the methodology outlined by (Mehta et al., 2022b). Cells were pelleted
128 from 15 mL of a culture grown to an optical density of 0.2, washed with MilliQ® water, dried
129 and ground in an agate mortar. Attenuated total reflectance Fourier transform infrared (ATR-
130 FTIR) spectra were acquired in the mid-IR region (4000–600 cm^{-1}) using a NICOLET 6700
131 FTIR spectrometer equipped with a diamond internal reflection element (IRE), a KBr beam
132 splitter and a deuterated triglycine sulfate (DTGS) detector. Spectra were collected by
133 averaging 64 scans at resolution of 4 cm^{-1}.
134

135 **2.3 Synchrotron-based X-ray absorption near edge structure (XANES) spectroscopy**

136 The relative quantification of Ca in iACC within *M. geothermalis* cells was achieved using
137 XANES spectroscopy, following the approach detailed by Mehta et al. (2023). For this, 15 mL
138 of a cell suspension were harvested by centrifugation, washed, and dried at 37 °C for 48 hours.
139 The dried biomass (~5 mg) was then diluted in 35 mg cellulose, pressed into a 10 mm diameter
140 pellet, and mounted onto Ca-free holders. XAS at the Ca K-edge was performed on the LUCIA
141 beamline at the SOLEIL synchrotron (Saint-Aubin, France) (Flank et al., 2006; Vantelon et al.,
142 2016). The fixed exit double-crystal monochromator was equipped with Si (111) crystals.
143 Spectra were recorded in the fluorescence mode using a 60 mm^2 mono-element silicon drift
144 diode detector (Bruker). In the pre-edge region (3940–4030 eV), spectra were recorded with a
145 step size of 2 eV and a counting time of 1 s. In the edge region (4030–4070 eV), spectra were
146 recorded with a step size of 0.25 eV and a counting time of 1 s. The sample holder was
147 positioned at a 24° angle relative to the fluorescence detector to minimize self-absorption
148 effects and was maintained at a temperature of 77 K using a liquid He-cryostat to minimize
149 potential beam damages and localized heating. Energy calibration was performed using a calcite
150 reference, with the first inflection point set to 4045 eV.

151

152 **2.4 Scanning electron microscopy (SEM)**

153 Cell suspensions of both *M. geothermalis* and *M. mesophilus* were filtered onto 0.22 µm Isopore
154 polycarbonate filters and rinsed with 10 mL of MilliQ® water. The filters were air-dried at
155 ambient temperature and mounted on aluminum stubs using double-sided carbon tape. Before
156 analysis, the filters were coated with a thin layer of carbon via evaporation. Scanning electron
157 microscopy (SEM) analyses were performed using a Zeiss™Ultra55 SEM with an electron
158 accelerating voltage of 10 kV, a working distance of 7.5 mm and a 60 µm aperture. Images
159 were captured using a backscattered electron detector (AsB detector). Energy-dispersive x-ray
160 spectrometry (EDXS) data were acquired with a Bruker QUANTAX EDS detector, enabling
161 hyperspectral imaging (HyperMap), and the data were analysed with the Esprit software
162 (Brucker).

163

164 **2.5 Transmission electron microscopy**

165 A 0.5 mL cell suspension was harvested by centrifugation, rinsed twice in 1 mL of MilliQ®
166 water before resuspension in 0.5 mL of MilliQ® water. A drop of 3 µL was deposited onto a
167 formvar-coated TEM grid and air-dried. Observations were carried out using a Jeol 2100F TEM
168 microscope operating at 200 kV, equipped with a Schottky emitter, a STEM device for Z-
169 contrast imaging in high-angular annular dark-field (HAADF) mode, and a Jeol Si(Li) X-ray
170 detector for elemental analyses via energy dispersive x-ray spectrometry (EDXS).

171

172 **2.6 Synchrotron-based cryo-soft X-ray tomography (c-SXT)**

173 Three-dimensional X-ray imaging of *M. geothermalis* cells was performed at the ALBA
174 synchrotron (Barcelona, Spain) using cryo-transmission X-ray microscopy at the MISTRAL
175 beamline (Sorrentino et al., 2015). The cryofixation process involved plunge-freezing at the
176 Institut Pasteur (Paris, France) using a Leica EM GP. A Quantifoil TEM grid (Q-R2/1-C2100)

177 was loaded in the chamber of the plunge freezer. Four microliters of a two-day-old *M.*
178 *geothermalis* culture (OD = 0.251) and one microliter of a 100-nm gold nanoparticles
179 suspension (BBI Solutions, 5X concentrated) were deposited on the front of the grid. After
180 blotting for four seconds from the back, grids were plunged into a container filled with liquid
181 ethane cooled with liquid nitrogen (-196°C), ensuring proper vitrification of the samples.
182 Subsequently, the samples were shipped from Paris to the ALBA synchrotron in a dry shipper
183 and transferred to the cryo-chamber of the Mistral beamline for imaging.
184 A tilt series of projections was collected from −70° to +70° in 1° increments (except otherwise
185 mentioned), with an incident X-ray energy of 520 eV. Each projection was exposed for 3
186 seconds. A 40-nm Fresnel zone plate was used, achieving an effective pixel size of 12 nm. The
187 projections were normalized for incoming flux and deconvolved using the measured point
188 spread function of the optical system (Otón et al., 2016). Projections were aligned using Etomo
189 with the 100-nm gold nanoparticle fiducials. Tomographic reconstruction, along with
190 simultaneous iterations reconstruction technique (SIRT) deconvolution, were performed using
191 IMOD (Otón et al., 2016). Volume segmentation, calculations and visualization of tomograms
192 were carried out using the Microscopy Image Browser and ImageJ (Belevich et al., 2016).
193

194 **2.7 Genome collection and phylogenomic analyses**

195 The 858 high-quality genome sequences of species of the order *Methyloccoccales* available in
196 the Genome Taxonomy Database (GTDB) version r220 (Parks et al., 2022) were downloaded.
197 They included seven families according to the GTDB taxonomy: *Cycloclasticaceae* (43
198 genomes), *Methylococcaceae* (112 genomes), *Methylomonadaceae* (679 genomes),
199 *Methylothermaceae* (13 genomes), UBA1147 (6 genomes), UBA2778 (3 genomes), and
200 DRLZ01 (2 genomes). Eight additional gammaproteobacterial genomes were downloaded to
201 serve as outgroup in phylogenomic analyses: *Coxiella burnetii* cb109 (GCA_000300315.1),

202 *Legionella pneumophila* Hextuple_2q (GCA_000277025.1), *Reinekea blandensis* MED297
203 (GCF_000153185.1), *Dichelobacter nodosus* (GCF_001263335), *Francisella tularensis*
204 FSC147 (GCA_000018925.1), *Nitrosococcus oceani* ATCC 19707 (GCF_000012805.1),
205 *Halorhodospira* sp. (GCA_007121755.1), and *Alkalilimnicola ehrlichii* MLHE-1
206 (GCF_000014785.1). Protein-coding genes were predicted with Prodigal (Hyatt et al., 2010)
207 when annotations were missing.
208 GTDB-Tk (Chaumeil et al., 2022) was used to identify 120 conserved protein markers encoded
209 in the whole collection of *Methylococcales* and outgroup genome sequences. Individual
210 markers were aligned using MAFFT L-INS-I v7.310 (Katoh et al., 2019). Poorly aligned sites
211 were removed using trimAl (Capella-Gutiérrez et al., 2009) with the –strictplus option and the
212 resulting trimmed alignments were concatenated using an in-house Python script, yielding an
213 alignment of 36,916 amino acid sites. A Maximum Likelihood tree based on this supermatrix
214 was inferred using IQ-TREE v3.0.1 (Wong et al., 2025) with the LG+G substitution model (Le
215 and Gascuel, 2008). Branch statistical support was calculated with 1,000 ultrafast bootstrap
216 replicates (Hoang et al., 2018). A tree including only the *Methylococcales* species containing
217 the *ccyA* gene was constructed using the same concatenated markers and the same method
218 described above.
219
220 **2.8 Detection of *ccyA***
221 The detection of *ccyA* was conducted using the in-house tool pCALF (standing for python
222 CALcyanin Finder, https://github.com/K2SOHIGH/pcalf/tree/main), which uses four hidden
223 Markov model (HMM) profiles describing the C-terminal glycine zipper triplication (called the
224 $(GlyZip)_3$ motif), specific of calcyanins in *Cyanobacteria* as described in detail by Gaschignard
225 et al. (2024).
226

227 **2.9 Sequence analysis**

228 Calcyanin protein sequences detected in *Methylococcales* were compared with those found in
229 *Cyanobacteria*. For this purpose, multiple sequence alignments were performed using MAFFT
230 L-INS-I v7.310 (Katoh et al., 2019), then checked and further analyzed using Hydrophobic
231 Cluster Analysis (HCA) (Bitard-Feildel et al., 2018). Aligned sequences were rendered on the
232 basis of ESPript 3.0 results (Gouet et al., 2003). 3D structure predictions were performed using
233 the AlphaFold3 server (Abramson et al., 2024).

234

235 **3. Results**

236

237 **3.1 Detection and phylogenetic distribution of *ccyA* in the order *Methylococcales***

238 The *ccyA* gene was identified as a diagnostic marker of iACC biomineralization in
239 *Cyanobacteria*. Moreover, homologs of *ccyA* were also reported in four gammaproteobacteria
240 of the order *Methylococcales* (Benzerara et al., 2022). To investigate this further, we
241 systematically searched for *ccyA* homologs across the 858 genome sequences of
242 *Methylococcales* species available in the Genome Taxonomy Database (GTDB) version r220
243 (Parks et al., 2022) (Table S1).

244 We detected *ccyA* in 39 genomes of species belonging to this order, distributed in the genera
245 *Methylococcus* (including *M. geothermalis* and *M. mesophilus*), *Methylospira* (*Candidatus*
246 Methylospira mobilis), and *Methylumidiphilus* (many strains affiliated with *M. alinensis*) (Table
247 1). According to the GTDB taxonomy, all these species were assigned to the family
248 *Methylococcaceae*; none were associated with the species-rich *Methylomonadaceae* or with the
249 other families of the order *Methylococcales* (Figure 1 and Figure S1). The species possessing
250 *ccyA* occur in diverse environments, including the water column and sediment of freshwater
251 lakes, compost, active municipal landfills, and rice field soils (Table 1 and Table S2). In all
252 identified genomes, the protein calcyanin was consistently annotated as a hypothetical protein.

According to the GTDB metadata, most of the genomes containing *ccyA* (34 out of 39) were metagenome-assembled genomes (MAGs), and only five originated from cultured isolates (Table 1). Only two of these isolates were available: *Methylococcus geothermalis* IM1 and *Methylococcus mesophilus* 16-5, which were used in our subsequent studies.

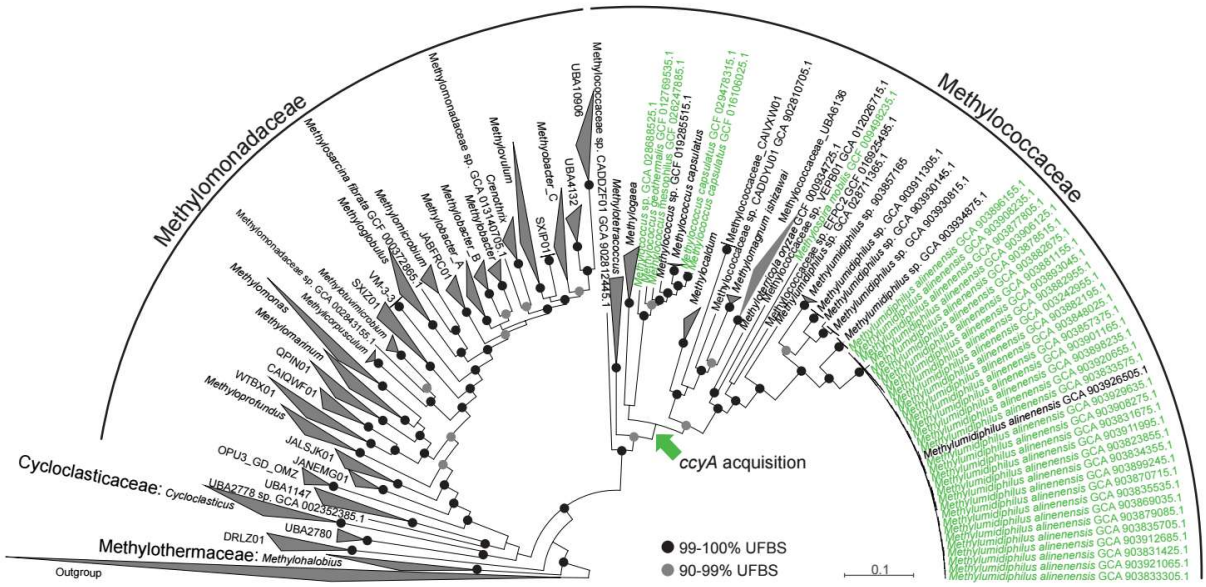

Figure 1: Maximum likelihood phylogenomic tree of 858 *Methylobacterales* taxa available in the Genome Taxonomy Database (GTDB version 220) (see Table S1). The tree is based on the concatenation of 120 conserved proteins. Taxa containing the *ccyA* gene are highlighted in green. Taxa that do not contain the *ccyA* gene are collapsed. Taxon names correspond to the GTDB taxonomy. The green arrow indicates the most likely point for the acquisition of *ccyA* by an ancestor of several *Methylococcaceae* lineages. Ultrafast bootstrap support (UFBS) values >90% are indicated on branches (black dots: 99-100%; gray dots: 90-99%). The complete, un-collapsed tree is available in Fig. S1.

Genome ID	Environmental biome	Geographic location	GTDB genus	Type	Strain availability	Bibliography
GCF_012769535.1	Geothermal environment	South Korea	*Methylococcus*	Isolate	Available axenic culture, *M. geothermalis*	Awala SI et al (2020)
GCF_016106025.1	Compost from a depth of 5 cm	Russia: Moscow region	*Methylococcus*	Isolate	No response from the person who isolated the strain	Patent RU2020129522A
GCF_026247885.1	Rice field soil; 10-15 cm deep	South Korea	*Methylococcus*	Isolate	Available axenic culture, *M. mesophilus*	Awala SI et al (2023)
GCF_029478315.1	Mixture of strains (e.g., ATCC 33009; BKM 2116) from several laboratories followed by selection under specific conditions	missing	*Methylococcus*	Isolate	*M. capsulatus* , No response from the person who isolated the strain	Patent RU2613365C1
GCF_009498235.1	Acidic Sphagnum-dominated peat bog	Russia: Tver region	*Methylospira*	Isolate	*Candidatus* Methylospira mobilis, strain was lost (pers. Comm. S. Dedysh)	Danilova OV et al. (2016).
GCA_028688525.1	landfill. NEUS_C leachate from a leachate well at an active municipal landfill in the North Eastern United States	USA	*Methylococcus*	MAG	NA	Grégoire et al. (2023). M
GCA_003242955.1	Stratified humic lake	Finland; Lake Alinen-Mustajarvi	*Methyloumidiphilus*	MAG	NA	Rissanen AJ, et al. (2018).
GCA_903912685.1	Lake sediment	Finland; Lake Alinen-Mustajarvi	*Methyloumidiphilus*	MAG	NA	Buck M et al. (2021)
GCA_903831675.1	Lake sediment	Finland; Lake Alinen-Mustajarvi	*Methyloumidiphilus*	MAG	NA	Buck M et al. (2021)
GCA_903831425.1	Lake sediment	Finland; Lake Alinen-Mustajarvi	*Methyloumidiphilus*	MAG	NA	Buck M et al. (2021)
GCA_903929635.1	Lake sediment	Finland; Lake Alinen-Mustajarvi	*Methyloumidiphilus*	MAG	NA	Buck M et al. (2021)
GCA_903882955.1	Lake water	Finland; Lake Alinen-Mustajarvi	*Methyloumidiphilus*	MAG	NA	Buck M et al. (2021)
GCA_903848025.1	Lake water	Finland; Lake Alinen-Mustajarvi	*Methyloumidiphilus*	MAG	NA	Buck M et al. (2021)
GCA_903896155.1	Lake water, Alinen Mustajärvi, 3m in depth	Finland; Lake Alinen-Mustajarvi	*Methyloumidiphilus*	MAG	NA	Buck M et al. (2021)
GCA_903921065.1	Lake water, Alinen Mustajärvi, 4.4m in depth	Finland; Lake Alinen-Mustajarvi	*Methyloumidiphilus*	MAG	NA	Buck M et al. (2021)
GCA_903908275.1	Lake water, Alinen Mustajärvi, 5.1m in depth	Finland; Lake Alinen-Mustajarvi	*Methyloumidiphilus*	MAG	NA	Buck M et al. (2021)
GCA_903899245.1	Lake water, Alinen Mustajärvi, 5.8m in depth	Finland; Lake Alinen-Mustajarvi	*Methyloumidiphilus*	MAG	NA	Buck M et al. (2021)
GCA_903834355.1	Lake water, Alinen Mustajärvi, 6.3 m in depth	Finland; Lake Alinen-Mustajarvi	*Methyloumidiphilus*	MAG	NA	Buck M et al. (2021)
GCA_903877805.1	Lake water, Alinen Mustajärvi, 3m in depth	Finland; Lake Alinen-Mustajarvi	*Methyloumidiphilus*	MAG	NA	Buck M et al. (2021)
GCA_903833575.1	Lake water, Alinen Mustajärvi, 4m in depth	Finland; Lake Alinen-Mustajarvi	*Methyloumidiphilus*	MAG	NA	Buck M et al. (2021)
GCA_903835705.1	Lake water, Alinen Mustajärvi, 5.5m in depth	Finland; Lake Alinen-Mustajarvi	*Methyloumidiphilus*	MAG	NA	Buck M et al. (2021)
GCA_903908235.1	Lake water, Alinen Mustajärvi, 6m in depth	Finland; Lake Alinen-Mustajarvi	*Methyloumidiphilus*	MAG	NA	Buck M et al. (2021)
GCA_903911995.1	Lake water, Alinen Mustajärvi, 4m in depth	Finland; Lake Alinen-Mustajarvi	*Methyloumidiphilus*	MAG	NA	Buck M et al. (2021)
GCA_903920655.1	Lake water, Alinen Mustajärvi, 4.5m in depth	Finland; Lake Alinen-Mustajarvi	*Methyloumidiphilus*	MAG	NA	Buck M et al. (2021)
GCA_903823855.1	Lake water, Alinen Mustajärvi, 4.5 m deep	Finland; Lake Alinen-Mustajarvi	*Methyloumidiphilus*	MAG	NA	Buck M et al. (2021)
GCA_903882195.1	Lake water, Alinen Mustajärvi, 5.5m in depth	Finland; Lake Alinen-Mustajarvi	*Methyloumidiphilus*	MAG	NA	Buck M et al. (2021)
GCA_903898235.1	Lake water, Alinen Mustajärvi, 6m in depth	Finland; Lake Alinen-Mustajarvi	*Methyloumidiphilus*	MAG	NA	Buck M et al. (2021)
GCA_903857375.1	Lake water, Alinen Mustajärvi, 3.5m in depth	Finland; Lake Alinen-Mustajarvi	*Methyloumidiphilus*	MAG	NA	Buck M et al. (2021)
GCA_903835535.1	Lake water, Alinen Mustajärvi, 4m in depth	Finland; Lake Alinen-Mustajarvi	*Methyloumidiphilus*	MAG	NA	Buck M et al. (2021)
GCA_903870715.1	Lake water, Alinen Mustajärvi, 4.5m in depth	Finland; Lake Alinen-Mustajarvi	*Methyloumidiphilus*	MAG	NA	Buck M et al. (2021)
GCA_903901165.1	Lake water, Alinen Mustajärvi, 5m in depth	Finland; Lake Alinen-Mustajarvi	*Methyloumidiphilus*	MAG	NA	Buck M et al. (2021)
GCA_903869035.1	Lake water, Alinen Mustajärvi, 5.5m in depth	Finland; Lake Alinen-Mustajarvi	*Methyloumidiphilus*	MAG	NA	Buck M et al. (2021)
GCA_903879085.1	freshwater sediment, Alinen Mustajärvi	Finland; Lake Alinen-Mustajarvi	*Methyloumidiphilus*	MAG	NA	Buck M et al. (2021)
GCA_903833305.1	freshwater sediment, Alinen Mustajärvi	Finland; Lake Alinen-Mustajarvi	*Methyloumidiphilus*	MAG	NA	Buck M et al. (2021)
GCA_903878515.1	Lake water, 3.9m in depth	Sweden; Lake Kiruna	*Methyloumidiphilus*	MAG	NA	Buck M et al. (2021)
GCA_903893045.1	Lake water, 4.2m in depth	Sweden; Lake Kiruna	*Methyloumidiphilus*	MAG	NA	Buck M et al. (2021)
GCA_903882675.1	Lake water	Sweden; Lake Kiruna	*Methyloumidiphilus*	MAG	NA	Buck M et al. (2021)
GCA_903881155.1	Lake water	Sweden; Lake Kiruna	*Methyloumidiphilus*	MAG	NA	Buck M et al. (2021)
GCA_903906125.1	Lake water, 0.2 m in depth	Sweden; Lake Bengtsgolen	*Methyloumidiphilus*	MAG	NA	Buck M et al. (2021)

Table 1: List of genomes of *Methylococcales* containing *ccyA*. Main information about the genomes, including whether they are derived from cultivated strain or metagenomes, the genera they are affiliated with following GTDB classification, their environmental and geographic origin.

3.2 Comparison of *Cyanobacteria* and *Methylococcaceae* calcyanin sequences

The calcyanin protein consists of two domains. The C-terminal $(GlyZip)_3$ domain, characterized by a triplicated long glycine zipper, is highly conserved across cyanobacteria (Benzerara et al., 2022). In contrast, the N-terminal domain is more variable and defines four calcyanin types called W (or CoBaHMA), X, Y and Z, the latter three being restricted to specific clades (*Gloeomargarita, Fischerella* and closely related genera, and *Microcystis*, respectively).

A multiple sequence alignment of the C-terminal domains revealed conservation of the signature motifs of the $(GlyZip)_3$ domain in the *Methylococcaceae* (Figure 2), which included the repeated basic Gly-X(3)-Gly pattern within each GlyZip motif, interrupted at the midpoint by a highly conserved Gly-Pro dipeptide. Additionally, several polar and aromatic amino acids were notably conserved, particularly in the third GlyZip motif. Some variability was observed among members of the *Methylococcaceae* as in the whole set of cyanobacteria sequences, which principally occurred outside the GlyZip motifs. Three-dimensional (3D) structure predictions using AlphaFold3 suggested that the GlyZip motifs form a hairpin structure of tightly packed alpha-helices, though predicted with low pLDDT confidence scores (Figure 3). Importantly, AlphaFold3 failed to accurately predict the spatial arrangement between these motifs, indicating that the $(GlyZip)_3$ domain may adopt an as-yet-unknown 3D fold.

These sequence comparisons further reveal that the *Methylococcaceae* C-terminal $(GlyZip)_3$ domains are more similar to Z-type calcyanins of *Microcystis* than to other types found in other cyanobacteria. Strong and specific sequence similarities are especially apparent in the first GlyZip motif (Figure 2). Additionally, *Microcystis* Z-type calcyanins and *Methylococcaceae* calcyanins also share features in their N-terminal domain, which lacks strongly hydrophobic amino acids and is enriched in alanine and polar residues (Fig. S2). However, despite these compositional similarities, no significant sequence alignments could be established between

these N-terminal sequences, which are predicted by AlphaFold3 to form coiled-coil structures, again with low confidence (Fig. S2).

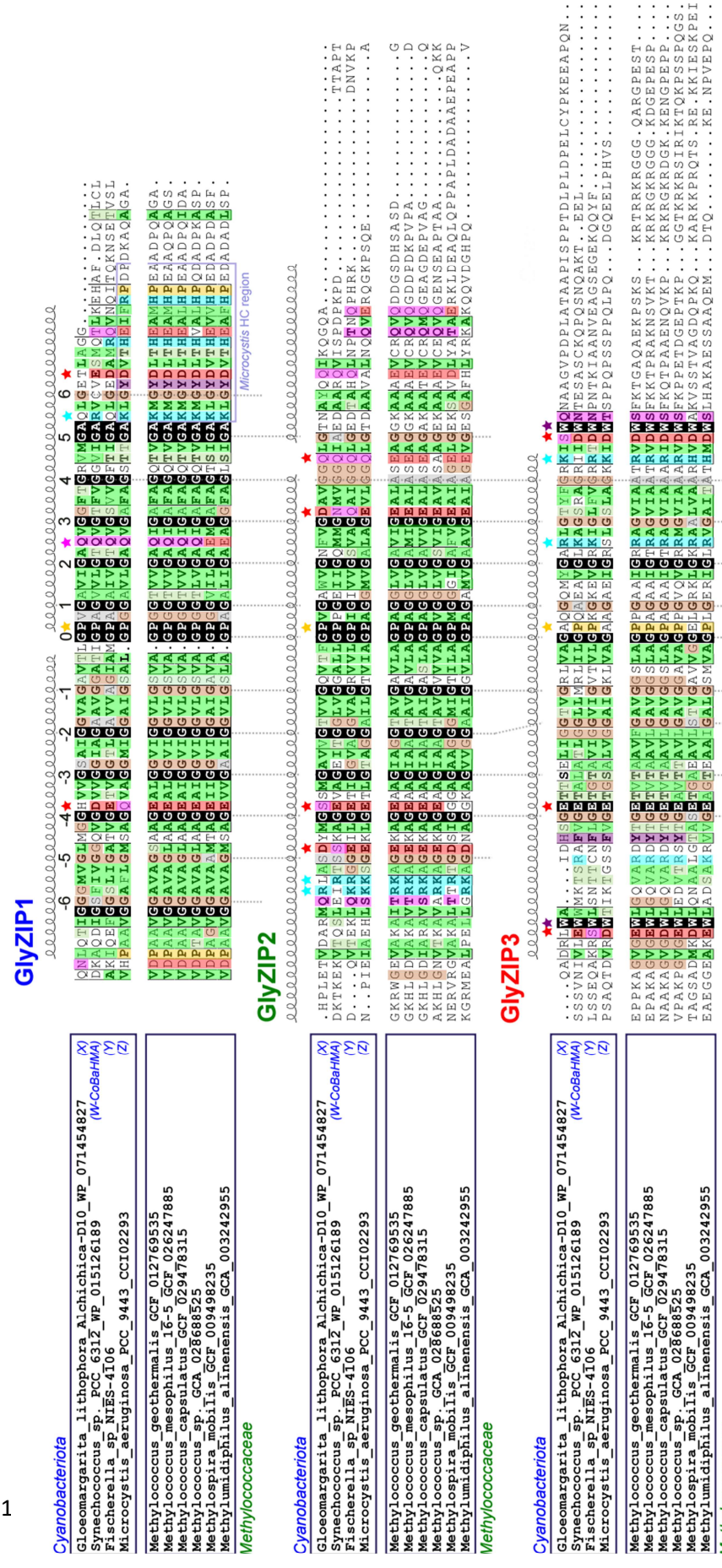

Figure 2: Comparison of the sequences of calcyanin GlyZip motifs of *Methylococcaceae* and cyanobacteria. Four calcyanin sequences representative of thmae different clades were selected for cyanobacteria, while for *Methylococcaceae*, six non-redundant ones were extracted from Table 1. The *Fischerella* sp. NIES-4106 calcyanin sequence was chosen as it has three GlyZip motifs, instead of two for most of the calcyanin sequences of this clade. Identities are shown in white on a black background, while similarities are highlighted with colors, according to amino acid properties and position in the alignment (with highly similar positions indicated in bold). The periodic motif involving glycine (or a small amino acid) every four residues is highlighted by numbers relative to the central conserved proline (gold star), and can be followed from one GlyZip motif to the next using vertical dotted lines. Highly conserved polar/aromatic positions are highlighted with stars. The lilac pink box highlights a region which is highly conserved (HC) between the *Microcystis* and *Methylococcaceae* sequences. The secondary structures (α-helices) as predicted by AlphaFold3 (pLDDT<70) on the *Methylococcus geothermalis* sequence are shown on top of the alignment.

Moreover, the similarity between the Z-type calcyanins of *Microcystis* and the new calcyanins of *Methylococcaceae* is strongly supported by phylogenetic analysis. Indeed, a maximum likelihood tree based on the GlyZip motifs conserved in the C-terminal domain of all calcyanins showed that the *Microcystis* and *Methylococcaceae* sequences are closely related with maximal statistical support (Figure 4). Interestingly, the relationships among the *Methylococcaceae* sequences perfectly mirrored those based on the phylogenomic analysis of a large set of conserved markers of the corresponding *Methylococcaceae* species (Figure 4), indicating that the *ccyA* gene has followed the speciation pattern of these species.

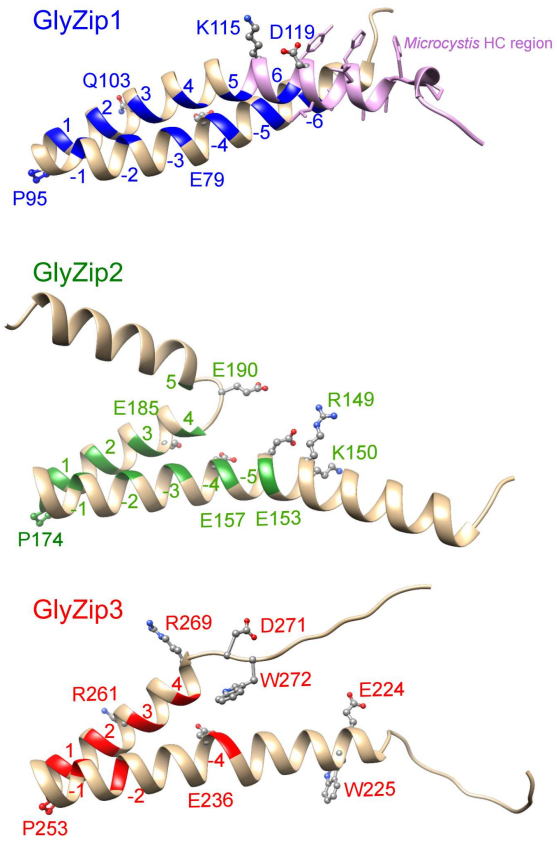

Figure 3: Ribbon representation of the 3D structure of the GlyZip motifs, as predicted by Alphafold3 using the *Methylococcus geothermalis* calcyanin sequence. The GlyZip motifs were superimposed with each other. The periodic motifs involving glycine (or a small amino acid) every four residues are colored on the ribbons, and highly conserved charged/polar/aromatic positions (stars in Figure 2) are depicted in atomic details. The region highly conserved (HC) between the *Microcystis* and *Methylococcaceae* sequences is highlighted in lilac pink. For note, the Alphafold3 per-residue pLDDT values are < 70, probably due to the fact that no template could be found in the protein data bank to support the relevance of this prediction (and not because of a dubious prediction, a hypothesis ruled out by in-depth analysis of the model, in particular highlighting the common central core around the Gly-Pro sequence). Structure uncertainties concern the more variable N- and C-terminal extremities of the GlyZip motifs, which in particular deviate from the packing imposed by the periodic repetitions of glycine in motifs 2 and 3.

Figure 4: Maximum likelihood phylogenetic tree of the GlyZip domain of the calcyanin sequences. Calcyanin sequences of *Methylococcaceae* species are highlighted in green. The different types of cyanobacterial calcyanins (X, W/CoBaHMA, Y, and Z) are indicated. For the *Methylococcaceae*, a species tree based on the concatenation of 120 conserved markers is shown on the left (this tree is rooted on an outgroup composed of *Methylococcaceae* sp. GCA_902812445.1, *Methylotetracoccus* sp. GCA_025458755.1, *Methylotetracoccus* sp. GCA_004168015.1, and *Methylotetracoccus oryzae* GCF 006175985.1). Numbers on branches show ultrafast bootstrap values. The sequences used the comparison of calcyanin sequences in Figure 2 appear in bold here.

357 **3.3 Experimental evidence of iACC formation by *Methylococcaceae* cultivated strains**

358 Both genomes of the cultivated strains *Methylococcus geothermalis* IM1 and *Methylococcus*
359 *mesophilus* 16-5 contain the *ccyA* gene, which is indicative of iACC formation in cyanobacteria.
360 Based on this, we searched for the presence of iACC in these strains. Laboratory cultures
361 exhibited a typical exponential growth curve, with a doubling time of 5.8±0.1 h for *M.*
362 *geothermalis* and 13.1±0.8 h for *M. mesophilus* (Fig. S3).

363 Attenuated total reflectance Fourier transform infrared (ATR-FTIR) spectroscopy performed
364 on cell pellets showed unambiguously the presence of ACC in both *Methylococcaceae*
365 cultivated strains (Figure 5 and Table S3 for band assignment). Indeed, spectra showed a band
366 at around 860 cm^{-1}, detected in both *M. geothermalis*, *M. mesophilus*, a synthetic ACC reference
367 and iACC-forming cyanobacteria but absent in a reference calcite and non-iACC-forming
368 cyanobacteria, and that was shown to be characteristic of ACC (Mehta et al., 2022b). Other
369 features observed in the spectra were bands at 1641 and 1528 cm^{-1}, identified as amide I and
370 amide II bands (Figure 5). Bands at 1444 and 1391 cm^{-1} detected in both *M. geothermalis* and
371 *M. mesophilus*, are similar to those observed at 1474 and 1395 cm^{-1} in ACC but they are not
372 exclusive to iACC-forming cyanobacteria and likely correspond to methyl groups in lipids
373 and/or C-O groups in carboxylic acids.

374 This finding was further corroborated by x-ray absorption near-edge structure (XANES)
375 spectroscopy at the Ca K-edge conducted on *M. geothermalis* cells. The derivative of the Ca K-
376 edge XANES spectrum of *M. geothermalis* cell pellets closely matched that of synthetic ACC
377 and iACC in cyanobacteria, distinguishing it from calcite and non-iACC-forming cyanobacteria
378 (Fig. 6; Mehta et al., 2023). Specifically, the B1 feature in the derivative spectrum, which was
379 shifted compared to calcite, indicated the presence of ACC. Linear combination fitting (LCF)
380 of the XANES data revealed that approximately ~57% of the Ca in *M. geothermalis* was in the

form of ACC, with the remaining 43% of Ca likely complexed by organics and/or associated with polyphosphates (Fig. 6).

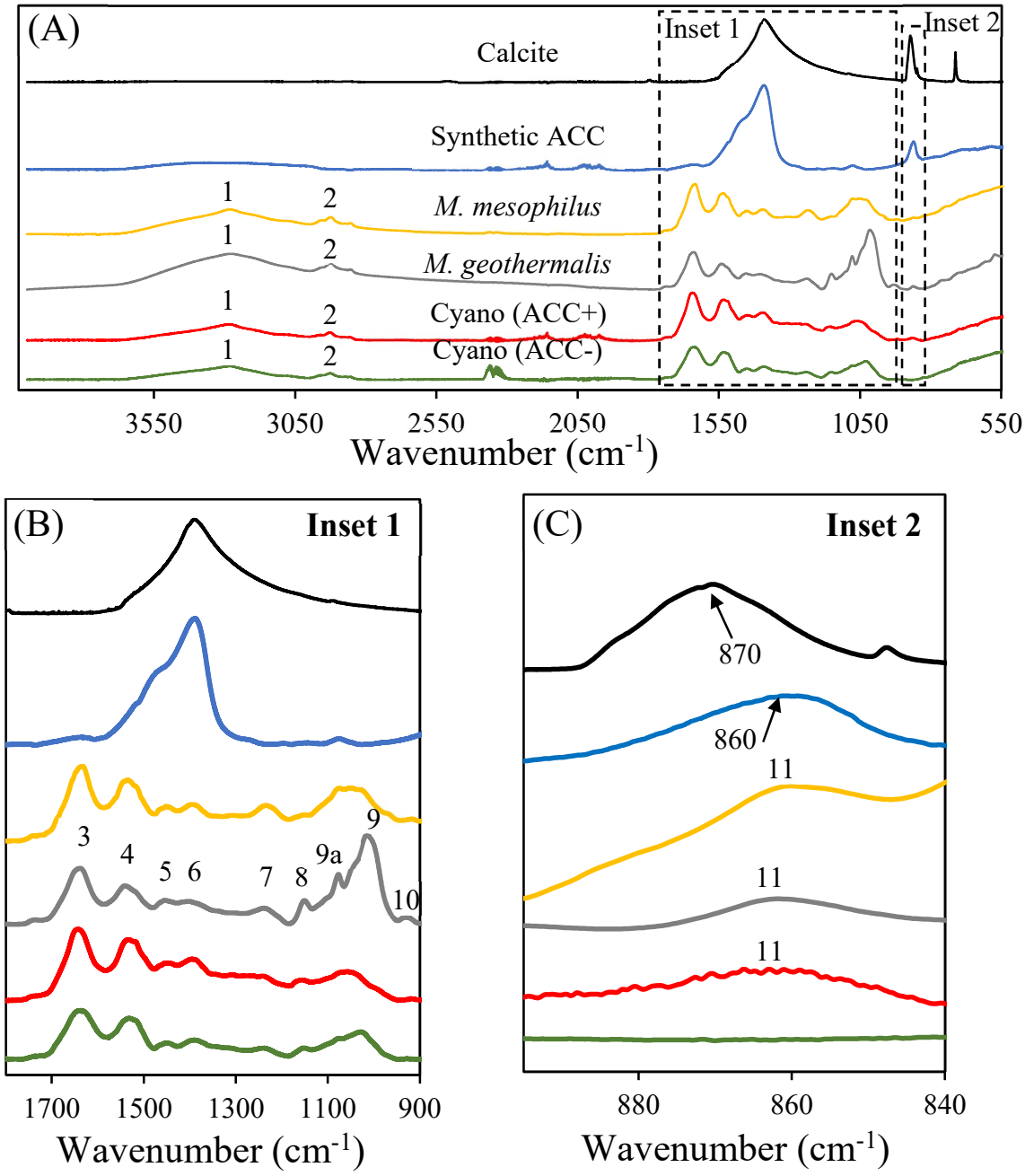

Figure 5: (A) ATR-FTIR spectra of *Methylococcus geothermalis* and *M. mesophilus* in the mid-IR range compared with reference spectra. Reference spectra are given for calcite, synthetic ACC, iACC-forming cyanobacteria (Cyano(ACC+)) and non-iACC-forming cyanobacteria (Cyano(ACC-)). The dashed rectangle envelops the zoomed regions of mid-IR ACC spectra shown in the inset 1 (1800–900 cm^{-1}) in (B), and inset 2 (950–820 cm^{-1}) in (C). Numbers on the spectra correspond to the band numbers and their assignment are provided in Table S3. Band 11 at 860 cm^{-1} is indicative of ACC.

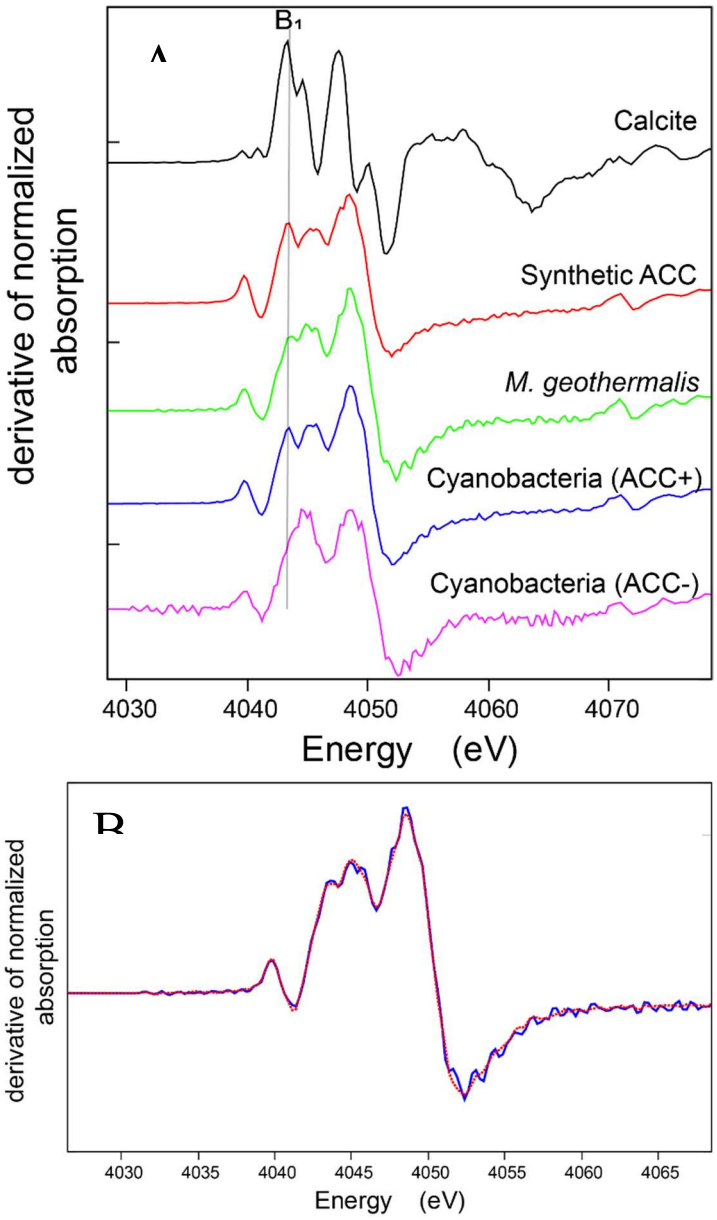

Figure 6: (A) Derivate XANES spectra at the Ca K-edge of *Methylococcus geothermalis* cell pellets compared with reference derivate spectra of calcite, synthetic ACC, iACC-forming cyanobacteria and non-iACC-forming cyanobacteria. The presence of a peak noted B1 indicated by a dashed line is indicative of ACC. (B) Linear combination fitting (LCF) of the derivate XANES spectrum of *Methylococcus geothermalis* cell pellets at the Ca K-edge. The solid line shows experimental data and the dotted line corresponds to the LCF result.

Consistently, both scanning electron microscopy (SEM) and scanning transmission electron microscopy (STEM) in the high-angle annular dark-field (HAADF) imaging mode combined with energy dispersive x-ray spectrometry (EDXS) showed that cells of both strains contained

Ca-rich inclusions with some Mg but no S and no P, interpreted as calcium carbonate inclusions (Fig. 7 and Fig. S4). Besides, cells also contained granules rich in phosphorus (P), with some Mg and K, interpreted as polyphosphate inclusions (Rivas-Lamelo et al., 2017).

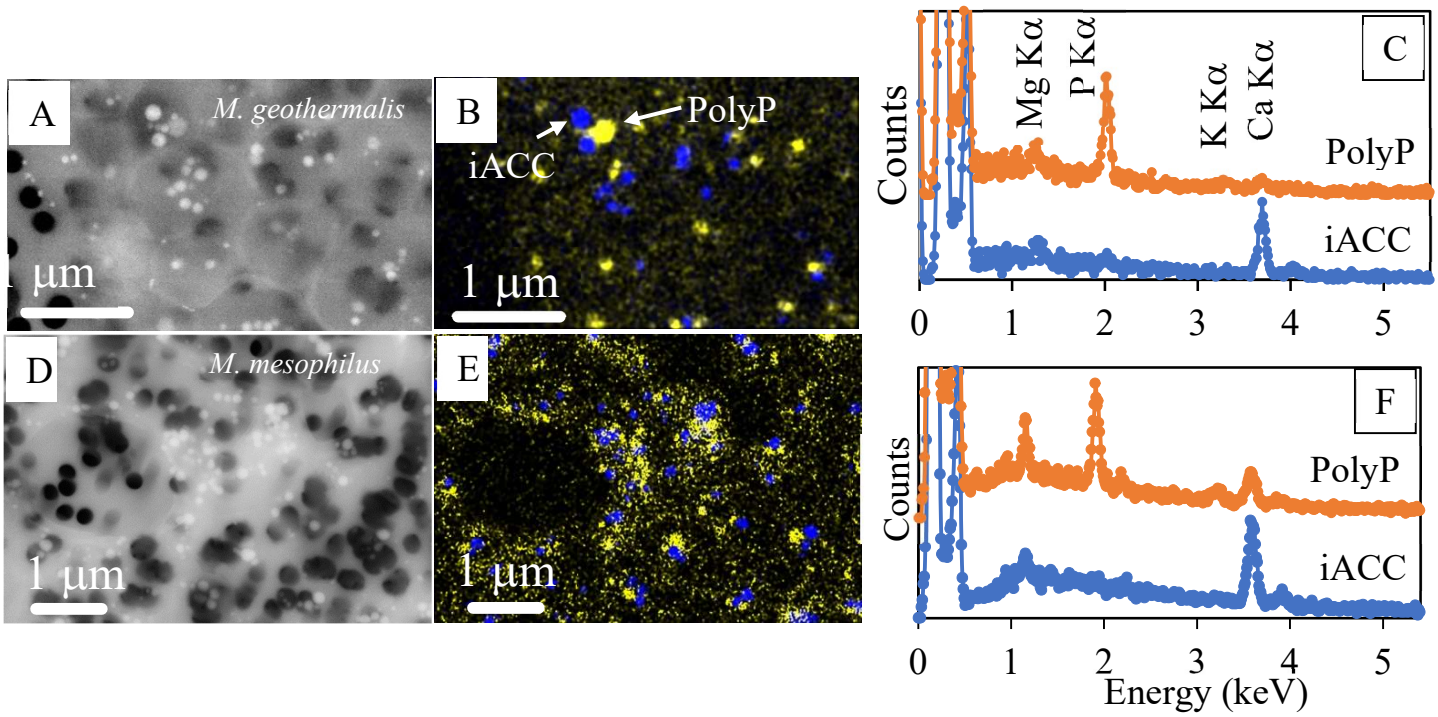

Figure 7: Scanning electron microscopy analyses of cultivated *Methylococcaceae*. (A-C) *Methylococcus geothermalis*. (A) Backscattered electron image. (B) Overlay of Ca (blue) and P (yellow) EDXS maps showing iACC and polyphosphate inclusions, respectively. (C) Characteristic EDXS spectra of polyphosphate (orange) and iACC (blue) inclusions. Emission lines of Mg Ka, P Ka, K Ka and Ca Ka are indicated. (D-F) Same analyses for *M. mesophilus*.

Last, cryo-soft X-ray tomography (c-SXT) was used to image vitrified *M. geothermalis* cells in a near-native state (15 cells in total, 6 cells used for volume reconstruction). Ca-rich inclusions were observed as regions of higher intensity (Figure 8A and Figure S5). These inclusions are most evident in the tomograms due to their strong absorption contrast and small, spherical morphology (Figure 8A). The absorption contrast from Ca-rich inclusions is much higher than other structures inside the cell (Figure 8B). Clearly defined Ca-rich inclusions were segmented to determine their average size and distribution, yielding a mean diameter of 118 ± 45 nm (n = 58) (Figure 8C). Other structural features, such as intracytoplasmic membranes and phosphate inclusions (Awala et al., 2020), can be distinguished from the smaller Ca-rich inclusions in the

tomograms but not from each other. For whole-cell segmentation, these structures were therefore grouped as a single material. Figure 8D shows the 3D volume reconstruction of the two cells from Figure 8A, highlighting the outer cell membrane, intracytoplasmic membranes/phosphate inclusions, and Ca-rich inclusions. At least 10 Ca-rich inclusions were found per cell.

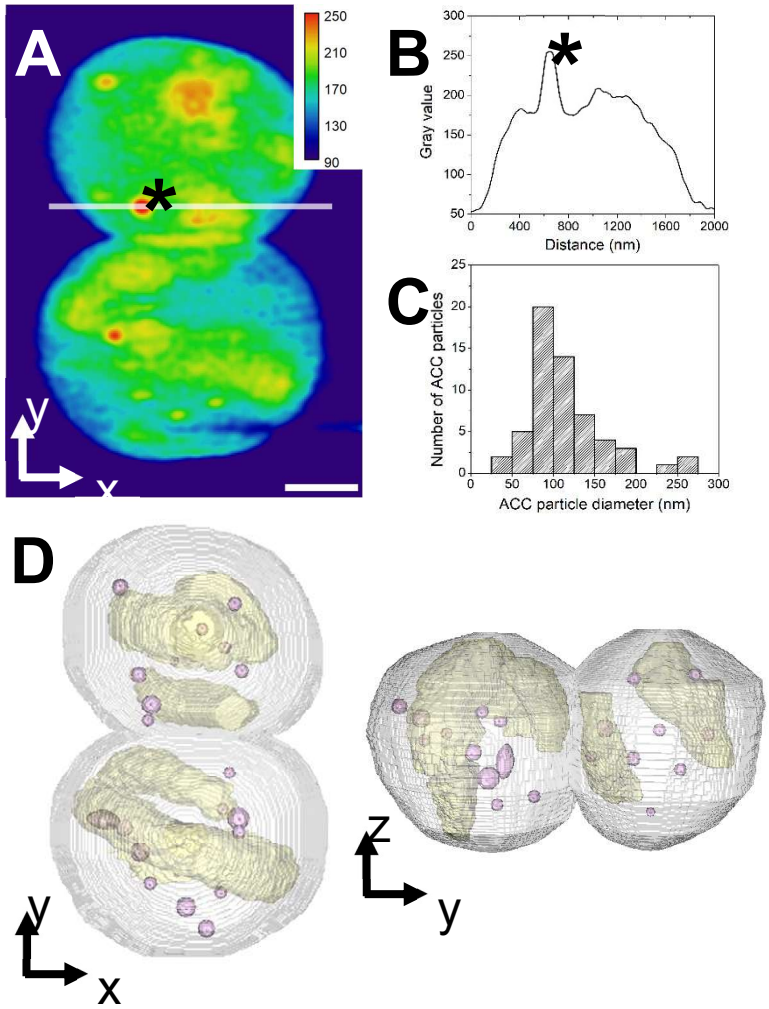

Figure 8: Cryo-soft X-ray tomography (c-SXT) of two ice-vitrified *Methylococcus geothermalis* cells. The image intensity corresponds to X-ray absorption by intracellular material at 520 eV—an energy within the "water window," where absorption by C and N atoms provides contrast of biological structures without chemical staining. At this energy, absorption by O atoms is minimal, allowing X-ray transmission through both the ice layer and hydrated cells. In contrast, the Ca $L_{2,3}$-edge at 350 eV enables detection of Ca atoms within the cells. (A) Virtual mid-cell z-slice of two *M. geothermalis* cells in reconstructed tomogram (an additional tomogram of two different cells is shown in Figure S3, along with tomogram videos for each dataset). Intensity scale (rainbow colour code) refers to absorption values. Asterisk marks position of a Ca-rich inclusion. Scale bar is 500 nm. (B) Absorption profile extracted from horizontal line in (A) (asterisk marks position of a Ca-rich inclusion). (C) Particle size distribution of Ca-rich granules measured from segmented volumes of the tomogram. (D) Volume reconstruction of cells in (A) shown in two perspectives with Ca-rich granules in pink, intracytoplasmic membranes/phosphate inclusions in beige and outer cell membrane in grey.

503 **4. Discussion**

504 **4.1 Formation of iACC inclusions by bacteria remains an overlooked process**

505 Here we report the discovery of iACC in members of the *Methylococcaceae*. This clade expands
506 the growing list of bacteria known to biomineralize ACC, which already includes *Achromatium*
507 (Benzerara et al., 2021; Gray, 2006; Schewiakoff, 1893), numerous phylogenetically diverse
508 members of the cyanobacteria (Benzerara et al., 2022) and several magnetotactic
509 *Pseudomonadota*, spanning both *Gammaproteobacteria* and *Alphaproteobacteria* (Liu et al.,
510 2021; Mangin et al., 2025; Monteil et al., 2020). Collectively, these discoveries suggest that
511 iACC biomineralization is more widespread than previously recognized but has often gone
512 unnoticed, likely due to the analytical challenges associated with detecting ACC. Indeed,
513 amorphous carbonates are highly labile and require dedicated techniques for reliable
514 identification (Addadi et al., 2003).

515 For example, although the ultrastructures of *M. geothermalis* and *M. mesophilus* had previously
516 been examined using electron microscopy, iACC granules were not reported (Awala et al.,
517 2020, 2023). This omission can be explained both by the distinct objectives of those studies
518 that did not targeted mineralogy and the absence of chemical analyses suited to the detection of
519 iACC. In contrast, our combined use of STEM-EDXS on intact, untreated cells together with
520 Ca K-edge XANES and/or FTIR spectroscopy enabled the unambiguous detection of iACC in
521 both species. Moreover, iACC granules were likely lost during the ultramicrotomy preparations
522 employed by Awala et al. (2020 & 2023) since standard protocols involving chemical fixation,
523 post-fixation and dehydration are known to dissolve iACC in cyanobacteria (Blondeau et al.,
524 2018a; Li et al., 2016). It is therefore possible that the numerous electron-translucent vesicles
525 or intracellular inclusions previously interpreted as polyphosphate or glycogen granules by
526 Awala et al. (2020, 2023) actually represent dissolved or transformed iACC granules. However,
527 this hypothesis can only be rigorously tested using cryo-electron microscopy of vitreous
528 sections (CEMOVIS).

529 An additional and pivotal line of evidence for iACC biomineralization in the *Methylococcaceae*
530 was the detection of the *ccyA* gene, previously identified as a diagnostic marker of iACC
531 formation in cyanobacteria (Benzerara et al., 2022). Our findings extend the diagnostic value
532 of *ccyA* beyond cyanobacteria, although so far, no other clades represented in current genomic
533 databases appear to carry this gene—unless their versions of *ccyA* have diverged substantially.
534 Importantly, however, the absence of *ccyA* does not necessarily imply the absence of iACC
535 formation. For instance, some magnetotactic *Pseudomonadota* and *Achromatium* both form
536 iACC despite lacking *ccyA*, suggesting that multiple, distinct molecular pathways may give rise
537 to iACC biomineralization (Mangin et al., 2025).
538 Last, numerous MAGs of iACC-forming *Methylococcaceae* that we have detected originate
539 from chemically stratified boreal lakes and ponds (Table 1; Buck et al., 2021). Interestingly,
540 MAGs from other bacteria phylogenetically close to iACC-forming magnetotactic bacteria
541 were also found in the same stratified lakes and ponds in Finland and Sweden (Mangin et al.,
542 2025), suggesting that iACC biomineralization might be a geochemically important process in
543 these lakes.
544

545 **4.2 Relationship between *Methylococcaceae* metabolism and iACC biomineralization**

546 The mechanisms governing iACC biomineralization remain poorly understood. It has been
547 proposed that bacterial primary metabolism may play an important role in driving this process
548 (Görgen et al., 2020). In *Achromatium*, a sulfur-oxidizing bacterium, iACC formation is linked
549 to sulfide oxidation to elemental sulfur (Yang et al., 2019). This reaction consumes protons,
550 thereby increasing intracellular pH. The resulting shift in carbonate equilibrium favors the
551 conversion of bicarbonate (HCO_3^-) to carbonate ions (CO_3^{2-}), which in turn promotes calcium
552 carbonate precipitation. Conversely, when elemental sulfur is oxidized to sulfate, protons are
553 released, decreasing intracellular pH and causing iACC dissolution. Thus, iACC function as a

554 dynamic pH buffer: consuming protons through their dissolution and releasing them through
555 their precipitation.
556 A similar hypothesis has been proposed for cyanobacteria, where photosynthesis elevates
557 intracellular pH and thereby increases carbonate ion concentration, favoring iACC precipitation
558 (Li et al., 2016). While these models hold for *Achromatium* and cyanobacteria, the present study
559 shows that a proton-consuming primary metabolism is not strictly required for iACC
560 biomineralization. In *Methylococcaceae*, aerobic methanotrophy does not consume protons, as
561 shown by equation (1):
562 $CH_4 + 2O_2 = CO_2 + 2H_2O$ (1)
563 Moreover, the CO_2 produced by aerobic methanotrophs should promote calcium carbonate
564 dissolution as shown by Krause et al. (2014) and according to carbonate equilibria:
565 $CaCO_3 + CO_2 + H_2O = Ca^{2+} + 2HCO_3^-$ (2)
566 However, a portion of this CO_2 may be diverted into small organic molecules via RuBiSCO-
567 mediated carbon fixation, as shown in *Methylococcus*, and may therefore not react with $CaCO_3$
568 (Oshkin et al., 2021). Overall, iACC precipitation in *Methylococcaceae* likely relies on an
569 additional, secondary metabolic process—yet to be identified—that consumes protons and
570 converts CO_2 into carbonate ions so that:
571 $CO_2 + H_2O = H_2CO_3$
572 $H_2CO_3 + Ca^{2+} + 2OH^- = CaCO_3 + 2H_2O$
573 Alternatively, if CO_2 fixation exceeds CO_2 release from methanotrophy, the net CO_2 production
574 by the cell would become at least sometimes negative, shifting the carbonate equilibrium
575 towards carbonate ions and favoring ACC precipitation. This hypothesis aligns with recent
576 findings in magnetotactic iACC-forming *Alphaproteobacteria*, whose primary metabolism
577 does not induce alkalinization but appears to support CO_2 fixation (Mangin et al., 2025).

578 Finally, calcium uptake is essential for storage within iACC. Ca^{2+}/H^{+} protein exchangers (Cax
579 proteins) are plausible candidates and we have detected *cax* genes in *Methylococcaceae*
580 genomes (data not shown). However, these transporters are generally inferred to function in
581 calcium efflux rather than uptake in bacteria (Waditee et al., 2004), which contradicts the
582 requirements for iACC formation. Future studies are needed to elucidate the specific metabolic
583 and transport processes enabling iACC biomineralization in *Methylococcaceae*. Aerobic
584 methane-oxidizing bacteria are widespread in many aquatic systems and have a significant
585 environmental and ecological role since they are key in the regulation of emissions of CH_4, a
586 potent greenhouse gas, and provide CH_4-derived organic carbon compounds to surrounding
587 heterotrophic microorganisms (Khanongnuch et al., 2022). How the capability to biomineralize
588 iACC in some of these organisms may play an overlooked regulatory role in these important
589 biogeochemical processes remains to be understood.
590
591 **4.3 Evolutionary origin of iACC biomineralization in *Methylococcaceae***
592 The *ccyA* gene has an ancient origin within cyanobacteria, explaining its broad phylogenetic
593 distribution across the phylum, with multiple secondary losses in modern lineages (Benzerara
594 et al., 2022). This evolutionary history gave rise to the diversification of several calcyanin
595 families, characterized by distinct N-terminal domains, termed CoBaHMA, X, Y, and Z. The
596 X, Y, and Z types are restricted to specific clades, i.e. *Gloeomargarita*, *Fischerella* (and closely
597 related genera), and *Microcystis*, respectively. In contrast, the CoBaHMA-type calcyanin
598 occurs in several distantly related lineages and has therefore been proposed as the most ancient
599 form of calcyanin.
600 The calcyanin sequences identified in *Methylococcaceae* have specific characteristics not found
601 in the four cyanobacterial types but share several similarities with the *Microcystis* (Z-type)
602 calcyanins. This is unexpected given the vast evolutionary distance between *Methylococcaceae*
603 and all the cyanobacterial clades. Phylogenetic analysis strongly supports the relationship

604 between the *Methylococcaceae* and cyanobacteria sequences (Figure 4). The most
605 parsimonious explanation for this observation is that *Methylococcaceae* acquired *ccyA* through
606 horizontal gene transfer (HGT) from a cyanobacterial ancestor closely related to *Microcystis*.
607 The fact that the phylogeny of the *Methylococcaceae* calcyanin sequences mirrors that of the
608 corresponding species, strongly suggests a single HGT acquisition by an ancestral
609 *Methylococcaceae* species, followed by subsequent divergence in several *Methylococcaceae*
610 subgroups, including many independent losses in the contemporary *Methylococcaceae* lineages
611 lacking *ccyA*. Such independent losses have also been proposed to explain the current
612 distribution of *ccyA* in the contemporary cyanobacteria lineages (Benzerara et al., 2022).
613 About 1/3 of known *Microcystis* genomes contain *ccyA*, which was also likely ancestral in this
614 genus and lost secondarily in several lineages (Gaetan et al., 2023). Consistently with the
615 presence of *ccyA*, abundant iACC-forming *Microcystis* strains have been observed in several
616 lakes (Gaetan et al., 2023). One plausible ecological setting for the HGT of *ccyA* from
617 *Microcystis* to *Methylococacceae* is exemplified by Lake Cadagno, a meromictic lake (i.e.,
618 permanently stratified with an anoxic monimolimnion). At its chemocline, methane removal is
619 driven by aerobic methane oxidizers which are physically associated with cyanobacteria
620 (Milucka et al., 2015). More precisely, physical associations between *Microcystis* and diverse
621 *Methylococcales* are common in lakes and ponds, where they may be responsible for an
622 overlooked sink for methane (Li et al., 2021). Similarly, microbial consortia comprising
623 cyanobacteria and methanotrophic bacteria are employed in oxygen-deficient wastewater
624 treatment plants to remove methane (Safitri et al., 2021). In these consortia, cyanobacteria
625 produce O_2 that fuels aerobic methanotrophy, while the resulting CO_2 is taken up by the
626 phototrophs. Such tight metabolic coupling provides an ideal setting for close and sustained
627 interactions between cyanobacteria and *Methylococcales*, potentially facilitating HGT. One of

these HGT events appears to have transmitted the capability to biomineralize iACC from cyanobacteria to *Methylococcaceae*.

Conclusions

This study shows that aerobic methanotrophs belonging to the *Methylococcaceae* family form iACC. They acquired the *ccyA* gene, a diagnostic marker of iACC biomineralization in cyanobacteria, through HGT from an ancestral *Microcystis*-like cyanobacterial donor. This HGT event may have taken place in a permanently stratified lake or in any other anoxic-oxic transition zone in aquatic habitats, where *Microcystis* and *Methylococcaceae* can co-exist. *Methylococcaceae* forming iACC may be abundant in some environments. Yet, how iACC are formed, in particular, how much of the carbon from methane oxidation is stored within iACC and diverted from the production of small organic carbon molecules by these bacteria remains to be quantified.

Data Availability Statement

All gene sequences were retrieved from GTDB as indicated in the Material and Method section and no new sequence was generated by this study. Microscopy and spectroscopy data are available on Zenodo reference number xxx.

Acknowledgements

This study was supported by the Agence Nationale de la Recherche (ANR), under grant Cyanoman, ANR-24-CE44-5543 and the ERC grants Calcyan (PI: K. Benzerara, Grant Agreement no. 307110). We thank synchrotron ALBA (Barcelona, Spain) for providing beamtime on the cryo transmission X-ray microscopy at the Mistral beamline under proposal number 2023027368. We thank synchrotron SOLEIL (Saclay, France) for providing beamtime to conduct XANES measurements on the LUCIA beamline under proposal number 20220623.

We also thank the IMPMC analytical platforms that enabled the data acquisition: Imène Estève for the SEM-EDXS support; Maxime Guillaumet and Keevin Beneut for IR spectroscopy support at IMPMC.

Conflict of interest statement

The authors declare no conflicts of interest.

Author contributions (see CRediT)

Benzerara Karim: conceptualization, formal analysis, writing – original draft, supervision, funding acquisition. **Millet Maxime**: conceptualization, methodology, formal analysis, writing – original draft. **Skouri-Panet Férial**: methodology, formal analysis, writing – review and editing. **Gaschignard Geoffroy**: methodology, formal analysis. **Mehta Neha**: methodology, formal analysis, writing – review and editing. **Bezard Malo**: formal analysis. **Caumes Geraldine**: conceptualization, formal analysis. **Chevrier Daniel M**.: formal analysis, writing – original draft. **Dezi Manuela**: funding acquisition. **Duverger Arnaud**: methodology. **Guigner Jean-Michel:** methodology. **Gutiérrez-Preciado Ana**: formal analysis. **Lefevre Christopher T**.: conceptualization, funding acquisition, writing – review and editing. **López-García Purificación**: conceptualization, funding acquisition, writing – review and editing. **Menguy Nicolas**: methodology. **Monteil Caroline L.**: conceptualization, funding acquisition, writing – review and editing. **Pehau-Arnaudet Gerard**: methodology. **Penard Esthel**: methodology. **Pereiro Eva**: methodology. **Scandola Cyril**: methodology. **Travert Cynthia**: methodology. **Vantelon Delphine**: methodology, writing – review and editing. **Duprat Elodie**: conceptualization, methodology, supervision, formal analysis. **Callebaut Isabelle**: conceptualization, methodology, formal analysis, supervision, writing – original draft. **Moreira**

David: conceptualization, methodology, formal analysis, supervision, writing – original draft, funding acquisition.

References

Abramson, J., Adler, J., Dunger, J., Evans, R., Green, T., Pritzel, A., Ronneberger, O., Willmore, L., Ballard, A. J., Bambrick, J., Bodenstein, S. W., Evans, D. A., Hung, C.-C., O'Neill, M., Reiman, D., Tunyasuvunakool, K., Wu, Z., Žemgulytė, A., Arvaniti, E., Beattie, C., Bertolli, O., Bridgland, A., Cherepanov, A., Congreve, M., Cowen-Rivers, A. I., Cowie, A., Figurnov, M., Fuchs, F. B., Gladman, H., Jain, R., Khan, Y. A., Low, C. M. R., Perlin, K., Potapenko, A., Savy, P., Singh, S., Stecula, A., Thillaisundaram, A., Tong, C., Yakneen, S., Zhong, E. D., Zielinski, M., Žídek, A., Bapst, V., Kohli, P., Jaderberg, M., Hassabis, D., and Jumper, J. M.: Accurate structure prediction of biomolecular interactions with AlphaFold 3, Nature, 630, 493–500, https://doi.org/10.1038/s41586-024-07487-w, 2024.

Addadi, L., Raz, S., and Weiner, S.: Taking advantage of disorder: amorphous calcium carbonate and its roles in biomineralization, Advanced Materials, 15, 959–970, https://doi.org/10.1002/adma.200300381, 2003.

Awala, S. I., Bellosillo, L. A., Gwak, J.-H., Nguyen, N.-L., Kim, S.-J., Lee, B.-H., and Rhee, S.-K.: *Methylococcus geothermalis* sp. nov., a methanotroph isolated from a geothermal field in the Republic of Korea, International Journal of Systematic and Evolutionary Microbiology, 70, 5520–5530, https://doi.org/10.1099/ijsem.0.004442, 2020.

Awala, S. I., Kim, Y., Gwak, J.-H., Seo, C., Lee, S., Kang, M., and Rhee, S.-K.: *Methylococcus mesophilus* sp. nov., the first non-thermotolerant methanotroph of the genus *Methylococcus*, from a rice field, International Journal of Systematic and Evolutionary Microbiology, 73, 006077, https://doi.org/10.1099/ijsem.0.006077, 2023.

Belevich, I., Joensuu, M., Kumar, D., Vihinen, H., and Jokitalo, E.: Microscopy Image Browser: A platform for segmentation and analysis of multidimensional datasets, PLOS Biology, 14, e1002340, https://doi.org/10.1371/journal.pbio.1002340, 2016.

Benzerara, K., Skouri-Panet, F., Li, J., Férard, C., Gugger, M., Laurent, T., Couradeau, E., Ragon, M., Cosmidis, J., Menguy, N., Margaret-Oliver, I., Tavera, R., López-García, P., and Moreira, D.: Intracellular Ca-carbonate biomineralization is widespread in cyanobacteria, PNAS, 111, 10933–10938, https://doi.org/10.1073/pnas.1403510111, 2014.

Benzerara, K., Bolzoni, R., Monteil, C., Beyssac, O., Forni, O., Alonso, B., Asta, M. P., and Lefevre, C.: The gammaproteobacterium *Achromatium* forms intracellular amorphous calcium carbonate and not (crystalline) calcite, Geobiology, 19, 199–213, https://doi.org/10.1111/gbi.12424, 2021.

Benzerara, K., Duprat, E., Bitard-Feildel, T., Caumes, G., Cassier-Chauvat, C., Chauvat, F., Dezi, M., Diop, S. I., Gaschignard, G., Görgen, S., Gugger, M., López-García, P., Millet, M., Skouri-Panet, F., Moreira, D., and Callebaut, I.: A new gene family diagnostic for intracellular biomineralization of amorphous Ca carbonates by cyanobacteria, Genome Biology and Evolution, 14, evac026, https://doi.org/10.1093/gbe/evac026, 2022.

Benzerara, K., Görgen, S., Athar, K. M., Chauvat, F., March, K., Menguy, N., Mehta, N., Skouri-Panet, F., Swaraj, S., Travert, C., Cassier-Chauvat, C., and Duprat, E.: Quantitative mapping of calcium cell

reservoirs in cyanobacteria at the submicrometer scale, Journal of Electron Spectroscopy and Related Phenomena, 267, 147369, https://doi.org/10.1016/j.elspec.2023.147369, 2023.

Bitard-Feildel, T., Lamiable, A., Mornon, J.-P., and Callebaut, I.: Order in disorder as observed by the "Hydrophobic Cluster Analysis" of protein sequences, Proteomics, 18, e1800054, https://doi.org/10.1002/pmic.201800054, 2018.

Blondeau, M., Sachse, M., Boulogne, C., Gillet, C., Guigner, J.-M., Skouri-Panet, F., Poinsot, M., Ferard, C., Miot, J., and Benzerara, K.: Amorphous calcium carbonate granules form within an intracellular compartment in calcifying cyanobacteria, Front. Microbiol., 9, 1768, https://doi.org/10.3389/fmicb.2018.01768, 2018a.

Blondeau, M., Benzerara, K., Ferard, C., Guigner, J.-M., Poinsot, M., Coutaud, M., Tharaud, M., Cordier, L., and Skouri-Panet, F.: Impact of the cyanobacterium *Gloeomargarita lithophora* on the geochemical cycles of Sr and Ba, Chemical Geology, 483, 88–97, https://doi.org/10.1016/j.chemgeo.2018.02.029, 2018b.

Bruley, A., Gaëtan, J., Gugger, M., Pancrace, C., Millet, M., Gaschignard, G., Dezi, M., Humbert, J.-F., Leloup, J., Skouri-Panet, F., Callebaut, I., Benzerara, K., and Duprat, E.: Diel changes in the expression of a marker gene and candidate genes for intracellular amorphous $CaCO_3$ biomineralization in *Microcystis*, Peer Community Journal, 5, https://doi.org/10.24072/pcjournal.516, 2025.

Buck, M., Garcia, S. L., Fernandez, L., Martin, G., Martinez-Rodriguez, G. A., Saarenheimo, J., Zopfi, J., Bertilsson, S., and Peura, S.: Comprehensive dataset of shotgun metagenomes from oxygen stratified freshwater lakes and ponds, Sci Data, 8, 131, https://doi.org/10.1038/s41597-021-00910-1, 2021.

Cam, N., Benzerara, K., Georgelin, T., Jaber, M., Lambert, J.-F., Poinsot, M., Skouri-Panet, F., Moreira, D., Lopez-Garcia, P., Raimbault, E., Cordier, L., and Jézéquel, D.: Cyanobacterial formation of intracellular Ca-carbonates in undersaturated solutions, Geobiology, 16, 49–61, https://doi.org/10.1111/gbi.12261, 2017.

Capella-Gutiérrez, S., Silla-Martínez, J. M., and Gabaldón, T.: trimAl: a tool for automated alignment trimming in large-scale phylogenetic analyses, Bioinformatics, 25, 1972–1973, https://doi.org/10.1093/bioinformatics/btp348, 2009.

Chaumeil, P.-A., Mussig, A. J., Hugenholtz, P., and Parks, D. H.: GTDB-Tk v2: memory friendly classification with the genome taxonomy database, Bioinformatics, 38, 5315–5316, https://doi.org/10.1093/bioinformatics/btac672, 2022.

Cosmidis, J. and Benzerara, K.: Why do microbes make minerals?, Comptes Rendus. Géoscience, 354, 1–39, https://doi.org/10.5802/crgeos.107, 2022.

Couradeau, E., Benzerara, K., Gerard, E., Moreira, D., Bernard, S., Brown, G. E., and Lopez-Garcia, P.: An early-branching microbialite cyanobacterium forms intracellular carbonates, Science, 336, 459–462, https://doi.org/10.1126/science.1216171, 2012.

Flank, A.-M., Cauchon, G., Lagarde, P., Bac, S., Janousch, M., Wetter, R., Dubuisson, J.-M., Idir, M., Langlois, F., Moreno, T., and Vantelon, D.: LUCIA, a microfocus soft XAS beamline, Nuclear Instruments and Methods in Physics Research Section B: Beam Interactions with Materials and Atoms, 246, 269–274, https://doi.org/10.1016/j.nimb.2005.12.007, 2006.

Gaetan, J., Halary, S., Millet, M., Bernard, C., Duval, C., Hamlaoui, S., Hecquet, A., Gugger, M., Marie, B., Mehta, N., Moreira, D., Skouri-Panet, F., Travert, C., Duprat, E., Leloup, J., and Benzerara, K.:

Widespread formation of intracellular calcium carbonates by the bloom-forming cyanobacterium *Microcystis*, Environmental Microbiology, 25, 751–765, https://doi.org/10.1111/1462-2920.16322, 2023.

Gilbert, P. U. P. A., Bergmann, K. D., Boekelheide, N., Tambutté, S., Mass, T., Marin, F., Adkins, J. F., Erez, J., Gilbert, B., Knutson, V., Cantine, M., Hernández, J. O., and Knoll, A. H.: Biomineralization: Integrating mechanism and evolutionary history, Science Advances, 8, eabl9653, https://doi.org/10.1126/sciadv.abl9653, 2022.

Görgen, S., Benzerara, K., Skouri-Panet, F., Gugger, M., Chauvat, F., and Cassier-Chauvat, C.: The diversity of molecular mechanisms of carbonate biomineralization by bacteria, Discov Mater, 1, 2, https://doi.org/10.1007/s43939-020-00001-9, 2020.

Gouet, P., Robert, X., and Courcelle, E.: ESPript/ENDscript: extracting and rendering sequence and 3D information from atomic structures of proteins, Nucleic Acids Res, 31, 3320–3323, https://doi.org/10.1093/nar/gkg556, 2003.

Gray, N. D.: The unique role of intracellular calcification in the genus *Achromatium*, in: Inclusions in Prokaryotes, edited by: Shively, J. M., Springer, Berlin, Heidelberg, 299–309, https://doi.org/10.1007/3-540-33774-1_11, 2006.

Hoang, D. T., Chernomor, O., von Haeseler, A., Minh, B. Q., and Vinh, L. S.: UFBoot2: Improving the Ultrafast Bootstrap Approximation, Mol Biol Evol, 35, 518–522, https://doi.org/10.1093/molbev/msx281, 2018.

Hyatt, D., Chen, G.-L., LoCascio, P. F., Land, M. L., Larimer, F. W., and Hauser, L. J.: Prodigal: prokaryotic gene recognition and translation initiation site identification, BMC Bioinformatics, 11, 119, https://doi.org/10.1186/1471-2105-11-119, 2010.

Katoh, K., Rozewicki, J., and Yamada, K. D.: MAFFT online service: multiple sequence alignment, interactive sequence choice and visualization, Brief Bioinform, 20, 1160–1166, https://doi.org/10.1093/bib/bbx108, 2019.

Khanongnuch, R., Mangayil, R., Svenning, M. M., and Rissanen, A. J.: Characterization and genome analysis of a psychrophilic methanotroph representing a ubiquitous *Methylobacter* spp. cluster in boreal lake ecosystems, ISME COMMUN., 2, 85, https://doi.org/10.1038/s43705-022-00172-x, 2022.

Le, S. Q. and Gascuel, O.: An improved general amino acid replacement matrix, Mol Biol Evol, 25, 1307–1320, https://doi.org/10.1093/molbev/msn067, 2008.

Li, C., Hambright, K. D., Bowen, H. G., Trammell, M. A., Grossart, H.-P., Burford, M. A., Hamilton, D. P., Jiang, H., Latour, D., Meyer, E. I., Padisák, J., Zamor, R. M., and Krumholz, L. R.: Global co-occurrence of methanogenic archaea and methanotrophic bacteria in *Microcystis* aggregates, Environmental Microbiology, 23, 6503–6519, https://doi.org/10.1111/1462-2920.15691, 2021.

Li, J., Margaret Oliver, I., Cam, N., Boudier, T., Blondeau, M., Leroy, E., Cosmidis, J., Skouri-Panet, F., Guigner, J.-M., Férard, C., Poinsot, M., Moreira, D., Lopez-Garcia, P., Cassier-Chauvat, C., Chauvat, F., and Benzerara, K.: Biomineralization patterns of intracellular carbonatogenesis in cyanobacteria: molecular hypotheses, Minerals, 6, 10, https://doi.org/10.3390/min6010010, 2016.

Liu, P., Liu, Y., Ren, X., Zhang, Z., Zhao, X., Roberts, A. P., Pan, Y., Li, J., and Semrau, J. D.: A novel magnetotactic Alphaproteobacterium producing intracellular magnetite and calcium-bearing

minerals, Applied and Environmental Microbiology, 87, e01556-21, https://doi.org/10.1128/AEM.01556-21, 2021.

Liu, P., Zhang, R., Meng, F., Zhang, C., Roberts, A. P., Wang, Y., Zhu, K., Cao, Z., Pan, Y., and Li, J.: Deep-branching magnetotactic bacteria form intracellular carbonates enriched in trace metals, mSystems, 0, e01131-25, https://doi.org/10.1128/msystems.01131-25, 2025.

Mangin, C. C., Benzerara, K., Bergot, M., Menguy, N., Alonso, B., Fouteau, S., Méheust, R., Chevrier, D. M., Godon, C., Turrini, E., Mehta, N., Duverger, A., Travert, C., Busigny, V., Duprat, E., Bolzoni, R., Cruaud, C., Viollier, E., Jézéquel, D., Vallenet, D., Lefèvre, C. T., and Monteil, C. L.: Magnetotactic bacteria affiliated with diverse *Pseudomonadota* families biomineralize intracellular Ca-carbonate, The ISME Journal, 19, wrae260, https://doi.org/10.1093/ismejo/wrae260, 2025.

Mehta, N., Benzerara, K., Kocar, B. D., and Chapon, V.: Sequestration of radionuclides Radium-226 and Strontium-90 by cyanobacteria forming intracellular calcium carbonates, Environ. Sci. Technol., 53, 12639–12647, https://doi.org/10.1021/acs.est.9b03982, 2019.

Mehta, N., Bougoure, J., Kocar, B. D., Duprat, E., and Benzerara, K.: Cyanobacteria accumulate Radium (226Ra) within intracellular amorphous calcium carbonate inclusions, ACS EST Water, 2, 616–623, https://doi.org/10.1021/acsestwater.1c00473, 2022a.

Mehta, N., Gaëtan, J., Giura, P., Azaïs, T., and Benzerara, K.: Detection of biogenic amorphous calcium carbonate (ACC) formed by bacteria using FTIR spectroscopy, Spectrochimica Acta Part A: Molecular and Biomolecular Spectroscopy, 278, 121262, https://doi.org/10.1016/j.saa.2022.121262, 2022b.

Mehta, N., Coutaud, M., Bouchez, J., van Zuilen, K., Bradbury, H. J., Moynier, F., Gorge, C., Skouri-Panet, F., and Benzerara, K.: Barium and strontium isotope fractionation by cyanobacteria forming intracellular carbonates, Geochimica et Cosmochimica Acta, 356, 165–178, https://doi.org/10.1016/j.gca.2023.07.014, 2023.

Mehta, N., Bradbury, H., and Benzerara, K.: Calcium isotope fractionation by intracellular amorphous calcium carbonate (ACC) forming cyanobacteria, Geobiology, 22, e12596, https://doi.org/10.1111/gbi.12596, 2024.

Milucka, J., Kirf, M., Lu, L., Krupke, A., Lam, P., Littmann, S., Kuypers, M. M., and Schubert, C. J.: Methane oxidation coupled to oxygenic photosynthesis in anoxic waters, ISME J, 9, 1991–2002, https://doi.org/10.1038/ismej.2015.12, 2015.

Monteil, C. L., Benzerara, K., Menguy, N., Bidaud, C. C., Michot-Achdjian, E., Bolzoni, R., Mathon, F. P., Coutaud, M., Alonso, B., Garau, C., Jézéquel, D., Viollier, E., Ginet, N., Floriani, M., Swaraj, S., Sachse, M., Busigny, V., Duprat, E., Guyot, F., and Lefevre, C. T.: Intracellular amorphous Ca-carbonate and magnetite biomineralization by a magnetotactic bacterium affiliated to the Alphaproteobacteria, The ISME Journal, 1–18, https://doi.org/10.1038/s41396-020-00747-3, 2020.

Oshkin, I. Y., Danilova, O. V., But, S. Y., Miroshnikov, K. K., Suleimanov, R. Z., Belova, S. E., Tikhonova, E. N., Kuznetsov, N. N., Khmelenina, V. N., Pimenov, N. V., and Dedysh, S. N.: Expanding characterized diversity and the pool of complete genome sequences of *Methylococcus* species, the bacteria of high environmental and biotechnological relevance, Front. Microbiol., 12, https://doi.org/10.3389/fmicb.2021.756830, 2021.

Otón, J., Pereiro, E., Pérez-Berná, A. J., Millach, L., Sorzano, C. O. S., Marabini, R., and Carazo, J. M.: Characterization of transfer function, resolution and depth of field of a soft X-ray microscope applied

to tomography enhancement by Wiener deconvolution, Biomed. Opt. Express, BOE, 7, 5092–5103, https://doi.org/10.1364/BOE.7.005092, 2016.

Pamart, E., Benzerara, K., Fois, G. R., Viola, S., Chauvat, F., Cassier-Chauvat, C., and Chapon, V.: Exploring the potential of *Gloeomargarita* lithophora for radionuclides bioremediation, JOURNAL OF HAZARDOUS MATERIALS, 492, https://doi.org/10.1016/j.jhazmat.2025.138155, 2025.

Parks, D. H., Chuvochina, M., Rinke, C., Mussig, A. J., Chaumeil, P.-A., and Hugenholtz, P.: GTDB: an ongoing census of bacterial and archaeal diversity through a phylogenetically consistent, rank normalized and complete genome-based taxonomy, Nucleic Acids Res, 50, D785–D794, https://doi.org/10.1093/nar/gkab776, 2022.

Ponce-Toledo, R. I., Deschamps, P., López-García, P., Zivanovic, Y., Benzerara, K., and Moreira, D.: An early-branching freshwater cyanobacterium at the origin of plastids, Current Biology, 27, 386–391, https://doi.org/10.1016/j.cub.2016.11.056, 2017.

Qin, W., Wang, C., Ma, Y., Shen, M., Li, J., Jiao, K., Tay, F. R., and Niu, L.: Microbe-mediated extracellular and intracellular mineralization: environmental, industrial, and biotechnological applications, Adv. Mater., 32, 1907833, https://doi.org/10.1002/adma.201907833, 2020.

Rivas-Lamelo, S., Benzerara, K., Lefèvre, C., Monteil, C., Jézéquel, D., Menguy, N., Viollier, E., Guyot, F., Ferard, C., Poinsot, M., Skouri-Panet, F., Trcera, N., Miot, J., and Duprat, E.: Magnetotactic bacteria as a new model for P sequestration in the ferruginous Lake Pavin, Geochemical Perspectives Letters, 5, 35–41, https://doi.org/10.7185/geochemlet.1743, 2017.

Safitri, A. S., Hamelin, J., Kommedal, R., and Milferstedt, K.: Engineered methanotrophic syntrophy in photogranule communities removes dissolved methane, Water Research X, 12, 100106, https://doi.org/10.1016/j.wroa.2021.100106, 2021.

Schewiakoff, W.: Uber einen neuen bakteriennähnlichen Organismus des Süßwassers, Habilitationsschrift, Heidelberg, 1893.

Sorrentino, A., Nicolás, J., Valcárcel, R., Chichón, F. J., Rosanes, M., Avila, J., Tkachuk, A., Irwin, J., Ferrer, S., and Pereiro, E.: MISTRAL: a transmission soft X-ray microscopy beamline for cryo nano-tomography of biological samples and magnetic domains imaging, J Synchrotron Rad, 22, 1112–1117, https://doi.org/10.1107/S1600577515008632, 2015.

Vantelon, D., Trcera, N., Roy, D., Moreno, T., Mailly, D., Guilet, S., Metchalkov, E., Delmotte, F., Lassalle, B., Lagarde, P., and Flank, A.-M.: The LUCIA beamline at SOLEIL, J Synchrotron Rad, 23, 635–640, https://doi.org/10.1107/S1600577516000746, 2016.

Waditee, R., Hossain, G. S., Tanaka, Y., Nakamura, T., Shikata, M., Takano, J., Takabe, T., and Takabe, T.: Isolation and functional characterization of Ca^{2+}/H^{+} antiporters from Cyanobacteria, J. Biol. Chem., 279, 4330–4338, https://doi.org/10.1074/jbc.M310282200, 2004.

Wan, J., Ji, R., Liu, J., Ma, K., Pan, Y., and Lin, W.: Biomineralization in magnetotactic bacteria: From diversity to molecular discovery-based applications, Cell Reports, 43, https://doi.org/10.1016/j.celrep.2024.114995, 2024.

Wong, T. K. F., Ly-Trong, N., Ren, H., Baños, H., Roger, A. J., Susko, E., Bielow, C., Maio, N. D., Goldman, N., Hahn, M. W., Huttley, G., Lanfear, R., and Minh, B. Q.: IQ-TREE 3: Phylogenomic inference software using complex evolutionary models, 2025.

Yang, T., Teske, A., Ambrose, W., Salman-Carvalho, V., Bagnell, R., and Nielsen, L. P.: Intracellular calcite and sulfur dynamics of *Achromatium* cells observed in a lab-based enrichment and aerobic incubation experiment, Antonie van Leeuwenhoek, 112, 263–274, https://doi.org/10.1007/s10482-018-1153-2, 2019.

Zhang, K., Tang, C.-S., Jiang, N.-J., Pan, X.-H., Liu, B., Wang, Y.-J., and Shi, B.: Microbial-induced carbonate precipitation (MICP) technology: a review on the fundamentals and engineering applications, Environ Earth Sci, 82, 1–33, https://doi.org/10.1007/s12665-023-10899-y, 2023.